ACS OMEGA

http://pubs.acs.org/journal/acsodf

Article

Au Nanoparticles Supported on Iron-Based Oxides for Soot Oxidation: Physicochemical Properties Before and After the Reaction

Chao Hu,* Zhenzhen Chen, Chao Wei, Xiaokang Wan, Wenzhi Li, and Qizhao Lin

Cite This: *ACS Omega* 2021, 6, 11510−11518

Read Online

ACCESS | Metrics & More | Article Recommendations

ABSTRACT: The catalytic performance of Au nanoparticles (NPs) supported on different transition-metal oxides for soot oxidation was studied in this paper. The changes in the morphology, phase structure, and physicochemical properties of Au-supported iron-based oxides before and after the reaction with soot particles were observed by high-resolution transmission electron microscopy, X-ray diffraction, X-ray photoelectron spectroscopy, and temperature-programed reduction. It was found that the catalytic activity of Fe_3O_4, Fe_2O_3, Co_3O_4, and NiO for soot oxidation was significantly improved after loading Au NPs. Especially, under the action of Au/Fe_2O_3 and Au/Fe_3O_4, the oxidation of soot was close to 20% below 420 °C, and their T_{10} values were 73 and 50 °C, respectively. When Au/Fe_2O_3 and Au/Fe_3O_4 reacted with soot, the size of the catalysts increased, and the active oxygen and Fe 2p components decreased. Au promoted the reduction of iron ions to a lower temperature, which was beneficial to improving the oxidation performance of iron-based oxides.

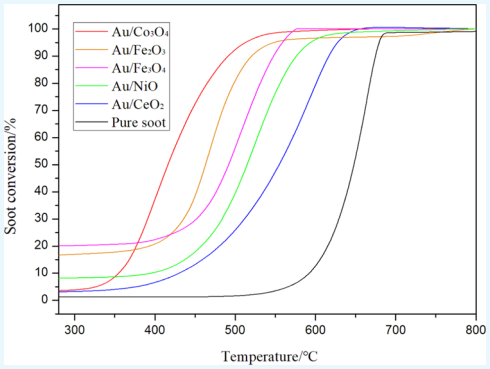

1. INTRODUCTION

Soot particles emitted from diesel engines can cause severe environmental and health problems.[1] For the elimination of soot particles, one of the most efficient after-treatment technologies is the use of a diesel particulate filter (DPF), in which particles are trapped.[2] However, soot deposition in DPF gradually increases the exhaust gas back pressure, resulting in a lower efficiency of the engine.[3] The loaded DPF needs to be regenerated by the combustion of soot deposits from the filter. The spontaneous combustion temperature of diesel soot is above 600 °C, while the temperature of the diesel exhaust gas is typically at 180−400 °C.[4] Thus, oxidative catalysts combined with the DPF to decrease the combustion temperature of soot is believed to be a feasible method in reducing soot emission.

The key to reducing the soot oxidation temperature is to find a suitable catalytic system. Recently, a series of catalysts such as noble metals, alkaline-metal oxides, transition-metal oxides, and perovskite oxides have shown good performances for soot oxidation.[5] Among the noble metals, Au catalysts have gained increasing attention because of their good catalytic activities in numerous reactions including the oxidation of volatile organic compounds, CO, and soot particles. In the catalytic combustion of methane, catalysts such as Au NPs loaded on La−Mn perovskites with a three-dimensional structure and Au−Pd loaded on Co_3O_4 show high performances, and the light-off temperature of methane can be achieved at 218 °C.[6,7] As for the catalytic oxidation of CO, supported Au NPs have been shown to be useful catalysts from the report of their high low-temperature oxidation activities by Hutchings' and Haruta's groups.[8,9] There have been a great number of studies on supported gold catalysts for CO oxidation. Recently, Zhang prepared a series of $Au/LaPO_4$ catalysts with good activity and stability and achieved complete CO conversion at 25 °C.[10]

Moreover, the gold catalysts have a great preference on the catalytic combustion of soot particles. Craenenbroeck et al. studied the catalytic activity of $Au-VO_x/TiO_2$ and $Au-VO_x/ZrO_2$ on diesel soot particles and found that the ignition temperature of soot was 361 °C and the peak burning temperature was 419 °C.[11] Au supported over ZnO is seen to be better than Ag/ZnO and CuO on soot particle oxidation, which is attributed to the stronger Coulombic force between Au^{3+} and soot.[12] Wei and Zhao's research group studied a series of catalysts with gold as the active component, including $Au/Ce_{0.8}Zr_{0.2}O_2$ and $AuPt/Ce_{0.8}Zr_{0.2}O_2$ alloy nanoparticles (NPs) and $Au@Pt/Ce_{0.8}Zr_{0.2}O_2$, $Au@CeO_{2-\delta}/ZrO_2$, and Au@

Received: February 2, 2021
Accepted: April 14, 2021
Published: April 26, 2021

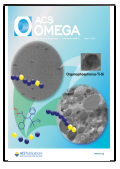

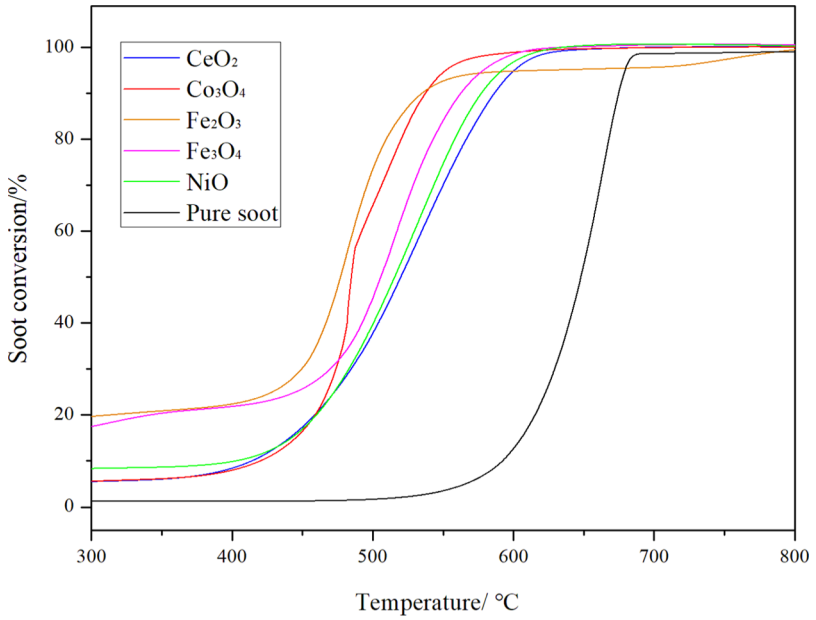

Figure 1. Catalytic performance of transition-metal oxides (CeO_2, Co_3O_4, Fe_2O_3, Fe_3O_4, and NiO) on soot particles.

La_2O_3 core−shell-structured NPs.[13−17] They observed that Au can significantly increase the active oxygen species on the surface of the catalyst and improve the catalytic activity.

The catalytic activity of Au NPs is related to a variety of factors, including the particle shape and size, oxide support materials, preparation procedures, oxygen supply pathways, coordination between Au NPs and support, and so forth.[18−20] Noble metals supported on oxides are typically deep oxidation catalysts. Strong metal−support interactions can exert dramatic influences on the catalytic performance of supported Au catalysts. The supports often play a key role in the process of catalytic reactions.[21] There are reducible oxide and irreducible oxide supports. The difference in the reducibility of these oxide can affect the properties of catalysts.[22] For example, Widmann observed that the catalytic activity for the oxidation of CO obeyed the sequence of Au/TiO_2 > Au/ZrO_2 > Au/ZnO > Au/Al_2O_3.[23] In the catalytic oxidation of ethyl acetate and toluene, Carabineiro concluded that Au/NiO and Au/CuO performed better than Au/Fe_2O_3, Au/MgO, and Au/LaO.[24] In the catalytic oxidation of toluene or propene, Liotta found that the oxidation activity decreased in the order of Au/CeO_2 >$Au/7.5Ce/Al_2O_3$ > Au/TiO_2 >Au/Al_2O_3.[25]

The activity of the catalyst for soot particle oxidation is related to its activation of oxygen and the contact opportunity between the catalyst and soot particles.[26] Au can promote the adsorption activation of oxygen molecules (O_2) and increase the number of active oxygen species (O_2^- and O_2^{2-}) on the catalyst surface.[27] Metal oxides are able to modify the catalytic property. One of the main catalytic functions of metal oxides in soot oxidation is to transfer the oxygen species from its surface to soot particles.[28] The spillover of oxygen and the subsequent chemical adsorption of active oxygen are the two important steps in the soot oxidation mechanism.[29] The role of the catalyst is to increase the transfer of active oxygen species to the surface of the soot, but it does not change the rate-determining step.[30] Their catalytic reactions depend largely on the electronic state of the metal oxide.[12] Moreover, transition-metal oxides display excellent redox properties due to the change in their valence state in the oxidation reactions. Metal ions can promote electrons to accumulate on the surface of the soot in a higher energy state, thereby enhancing the driving force to effectively transfer electrons from the soot to O_2.[31] The oxygen spillover and the election-transfer mechanisms complement each other in the oxidation reaction of soot with the catalyst.

High-resolution transmission electron microscopy (HRTEM), X-ray diffraction (XRD), and Fourier transform infrared (FTIR) spectroscopy are often used to investigate the changes in the soot morphology and reactivity.[32] Ambient-pressure X-ray photoelectron spectroscopy (AP-XPS) is constantly used to study the chemically bonded species on the catalyst surfaces and the molecular interaction between the catalyst and adsorbates under reaction conditions.[33,34] The aim of this work is to study the catalytic performances and the intrinsic activity of the transition-metal-oxide-supported gold catalysts for soot oxidation. A series of catalysts of Au/oxide (oxide = Fe_2O_3, Fe_3O_4, Co_3O_4, NiO, and CeO_2) were designed and successfully synthesized by the deposition−precipitation method. Especially, the structures, electronic properties, and reduction of catalysts Au/Fe_2O_3 and Au/Fe_3O_4 were investigated before and after the reaction with soot particles. The catalysts were investigated using HRTEM, XRD, X-ray photoelectron spectroscopy (XPS), and temperature-programed hydrogen reduction (H_2-TPR). Using these properties of the catalysts, the nature of the interactions between iron-based oxides and Au NPs was also investigated.

2. RESULTS AND DISCUSSION

2.1. Catalytic Performances of Transition-Metal Oxides for Soot Oxidation. The catalytic performance of variable valence transition-metal oxides without Au NPs for soot oxidation is first studied, and the results are shown in Figure 1. The pure soot had almost no oxidation below 550 °C, and its initial oxidation temperature T_{10} was 592 °C. The oxidation rate of the soot reached the highest at 600−700 °C, and the complete oxidation was achieved near 700 °C. The five transition-metal oxide catalysts studied in this paper, Fe_2O_3, Fe_3O_4, Co_3O_4, NiO, and CeO_2, can oxidize the soot particles at

https://doi.org/10.1021/acsomega.1c00619
ACS Omega 2021, 6, 11510−11518

the temperature of 400−450 °C. 450−600 °C was the main temperature range of the catalytic oxidation of soot particles, which were almost completely oxidized before 600 °C. It can be seen that the transition-metal oxide can effectively reduce the oxidation temperature of soot particles, so that the complete conversion temperature can be reduced by at least 100 °C. Among them, Fe_2O_3 had the best ability to catalyze the oxidation of the soot, its initial oxidation temperature was 450 °C. The temperature corresponding to its maximum conversion rate was 492 °C, and the burnout temperature was 535 °C; the complete conversion temperature of the soot decreased by 150 °C. The order of the catalytic oxidation activity of these five variable valence transition-metal oxide catalysts to soot particles is: Fe_2O_3 > Co_3O_4 > Fe_3O_4 >NiO > CeO_2. Fe_2O_3 and Fe_3O_4 iron-based catalysts show good catalytic activity in soot oxidation.

The conversion rate of Fe_2O_3 and Fe_3O_4 for soot particle oxidation before 420 °C is close to 20%, but the conversion curve is smooth. For Fe_2O_3, the curve starts to steepen at 445 °C, then increases rapidly; for Fe_3O_4, the conversion rate gradually increased at 471 °C. The probability of soot particles starting to oxidize is relatively small before 420 °C; the conversion curve above zero indicates that the soot particles have a physical reaction rather than an oxidation reaction with the iron-based catalyst. The iron-based catalyst begins to oxidize soot particles after 445 °C.

In order to characterize the catalytic activity of these catalysts on soot particles more directly and accurately, the characteristic temperatures T_{10}, T_{50}, T_{90}, and T_m of the catalytic reaction are summarized, as shown in Table 1. By comparing the relationship between the characteristic temperatures of different catalysts, the catalytic activity can be easily judged, the lower the characteristic temperature, the stronger the catalytic activity. The T_{10} of Fe_2O_3 and Fe_3O_4 are 87 and 100 °C, respectively.

Table 1. Characteristic Temperatures of Different Transition-Metal Oxides (CeO_2, Co_3O_4, Fe_2O_3, Fe_3O_4, and NiO) for the Catalytic Reaction of Soot Particles

	characteristic temperature (°C)			
catalyst	T_{10}	T_{50}	T_{90}	T_m
CeO_2	413	520	586	528
Co_3O_4	420	485	537	487
Fe_2O_3	87	477	535	492
Fe_3O_4	99	505	562	522
NiO	402	515	577	541
soot	592	648	674	662

2.2. Catalytic Performances of Au/Oxide for Soot Oxidation. The transition-metal oxide catalyst supported by Au NPs was prepared by the DP method. The catalyst and soot particles were mixed and ground to form a mixture, which was then subjected to thermogravimetric analysis. According to the soot quality change and the calculation formula of the soot conversion rate, the conversion efficiency of soot particles with different catalysts is obtained, as shown in Figure 2. According to the temperature value corresponding to the conversion efficiency, the conversion characteristic temperatures of soot particles oxidation are summarized in Table 2.

As can be seen from Figure 2, the Au-supported transition-metal oxide catalyst can further reduce the oxidation temperature of soot particles, but the effects of catalysts with different supports in reducing the oxidation temperature of soot particles are different. In general, the initial oxidation temperature of soot particles on Au/CeO_2, Au/Co_3O_4, Au/Fe_2O_3, Au/Fe_3O_4, and Au/NiO was 350−450 °C, and the main reaction temperature range was 400−600 °C; the soot particles basically burned out after 600 °C.

Comparing Figures 1 and 2, it can be found that the catalytic activity of the transition-metal oxide has changed after loading with Au NPs. For example, after the catalyst Co_3O_4 was loaded with Au NPs, its initial oxidation temperature of soot particles decreased from 420 to 354 °C, the burnout temperature decreased from 537 to 491 °C, and the characteristic temperature of the maximum combustion rate decreased from 487 to 395 °C. The catalytic activity of Co_3O_4 was improved after loading Au NPs. However, for the catalyst CeO_2, its catalytic activity decreased after Au NPs were supported. The initial oxidation temperature of soot increased from 413 to 430 °C, the burnout temperature increased from 586 to 616 °C, and the characteristic temperature of the maximum combustion rate increased from 528 to 582 °C. For the catalysts Fe_2O_3, Fe_3O_4, and NiO after loading with Au NPs, their initial temperature, burnout temperature and maximum combustion rate characteristic temperature had all decreased, which means that Au NPs increased their catalytic oxidative activity of soot particles. The order of the activity capacity of Au-loaded transition-metal oxides for the catalytic oxidation of soot particles was: Au/Co_3O_4 > Au/Fe_2O_3 > Au/Fe_3O_4 > Au/NiO > Au/CeO_2. Au/Fe_2O_3 and Au/Fe_3O_4 show good catalytic oxidation activity after loading Au NPs.

Interestingly, catalysts Au/Fe_2O_3 and Au/Fe_3O_4 had a conversion efficiency of nearly 20% for soot particles before 400 °C, but the conversion curves were always relatively smooth. For Au/Fe_2O_3, the conversion curve began to steepen at 425 °C and the soot conversion rate gradually increased. For catalyst Au/Fe_3O_4, the conversion rate of soot particles began to increase slowly at 441 °C. The T_{10} of Au/Fe_2O_3 and Au/Fe_3O_4 are 73 and 50 °C, respectively. For catalysts Au/Fe_2O_3 and Au/Fe_3O_4, the possibility of the catalytic oxidation of soot particles before 425 °C is very small. Therefore, we believe that the conversion efficiency of soot particles is nearly 20% mainly due to the physical reaction between the soot particles and iron-based catalyst, whose mechanism needs further experimental study.

2.3. Characterization of the Catalysts before and after the Reaction with Soot Particles. Characterizing of the structure and properties of the catalysts before and after the reaction with soot particles will help us to understand the physicochemical properties of the catalyst and the catalytic oxidation mechanism of soot particles more clearly.

Figure 3 shows the TEM images of Au/Fe_3O_4 before and after the reaction with soot particles. Before the reaction, Au NPs were small, spherical, and relatively dispersed, and Fe_3O_4 was large in size and forms a block structure. Au NPs were well attached to the surface of Fe_3O_4. The average diameter of Au NPs was 11.2 nm before the reaction and was 17.4 nm after the reaction. Their size distribution is shown in Figure 4. The increase in the size of Au NPs may be due to the slight sintering and aggregation after the reaction between the catalyst and soot particles at 400 °C. These small Au NPs agglomerated to form a larger particle, but they were not sintered to form a block structure.

Figure 5a,b shows the high-resolution electron microscopy images of catalyst Au/Fe_3O_4 before and after the reaction with

https://doi.org/10.1021/acsomega.1c00619
ACS Omega 2021, 6, 11510−11518

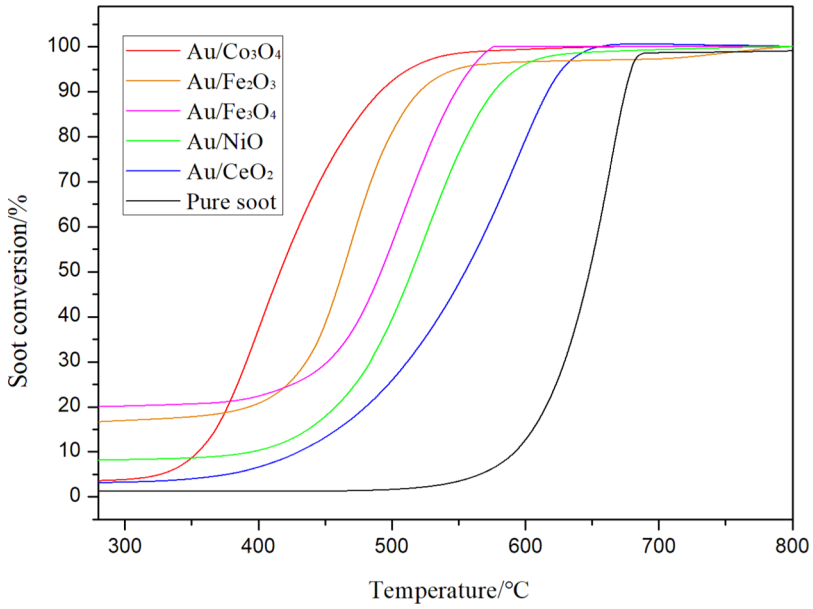

Figure 2. Catalytic performance of Au/Oxide (oxide = CeO_2, Co_3O_4, Fe_2O_3, Fe_3O_4, and NiO) on soot particles.

Table 2. Characteristic Temperature of Catalytic Oxidation of Au/Oxide with Soot Particles (Oxide = Co_3O_4, Fe_2O_3, Fe_3O_4, NiO, and CeO_2)

	characteristic temperature (°C)			
catalyst	T_{10}	T_{50}	T_{90}	T_m
Au/CeO_2	430	554	616	582
Au/Co_3O_4	354	416	491	395
Au/Fe_2O_3	73	463	520	474
Au/Fe_3O_4	50	491	548	495
Au/NiO	395	514	576	531

soot particles, respectively. It can be calculated from the figure that the lattice spacing of Fe_3O_4 is 0.316 nm, which is consistent with the lattice spacing of Fe_3O_4 (220) of 0.30 nm.[35] The lattice spacing of Au is 0.273 nm, which is close to 0.24 nm of Au (111).[36] The crystal structure with a lattice spacing of 0.278 nm can be measured from the high-resolution electron microscope image of the catalyst after the reaction with soot particles, which is more consistent with the lattice spacing of Fe_2O_3 (104) of 0.27 nm.[37]

The catalyst Au/Fe_3O_4 after the reaction with soot particles is studied by EDS analysis, as shown in Figure 6. It indicates the existence of Fe and Au in the catalyst. Cu from the TEM grid has the highest peak. Because the loading content of Au in the catalyst Au/Fe_3O_4 was low, the peak of Au is relatively small and the peak of Fe is relatively high. The peak corresponding to oxygen in the catalyst can also be seen from the figure.

Figure 7 shows the XRD spectra of the catalysts Au/Fe_2O_3 and Au/Fe_3O_4 before and after the reaction with soot particles. Au/Fe_2O_3 and Au/Fe_3O_4 showed characteristic diffraction peaks of α-Fe_2O_3 at 2θ = 24.1, 33.2, 35, 41, 49, 54, and 62° (PDF 00-033-0664), and the characteristic diffraction peaks of Au (PDF 00-065-2870) appear at 2θ = 38, 44, and 77°. In addition, the characteristic diffraction peaks (PDF 00-019-0629) of γ-Fe_2O_3 (400) appearing at 2θ = 30 and 43.5° were observed in the XRD spectra of Au/Fe_3O_4 before and after the reaction with soot particles. In the XRD pattern of the Au/Fe_3O_4 catalyst, the characteristic diffraction peaks of α-Fe_2O_3 and γ-Fe_2O_3 simultaneously appeared, indicating the coexistence of the two phases because γ-Fe_2O_3 can be converted into α-Fe_2O_3 when heated over 300 °C in the air.[38]

Before the soot oxidation reaction, the number of characteristic diffraction peaks of the catalysts was small and the peak width was large. This is due to the small nanometer size of the catalysts particles before the reaction, which leads to a large half-peak width. According to the Scherrer equation, the larger

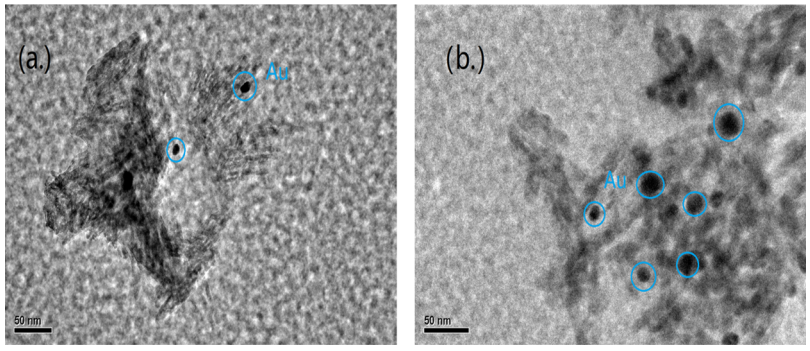

Figure 3. TEM images of Au/Fe_3O_4 before (a) and after (b) reaction with soot particles.

https://doi.org/10.1021/acsomega.1c00619
ACS Omega 2021, 6, 11510−11518

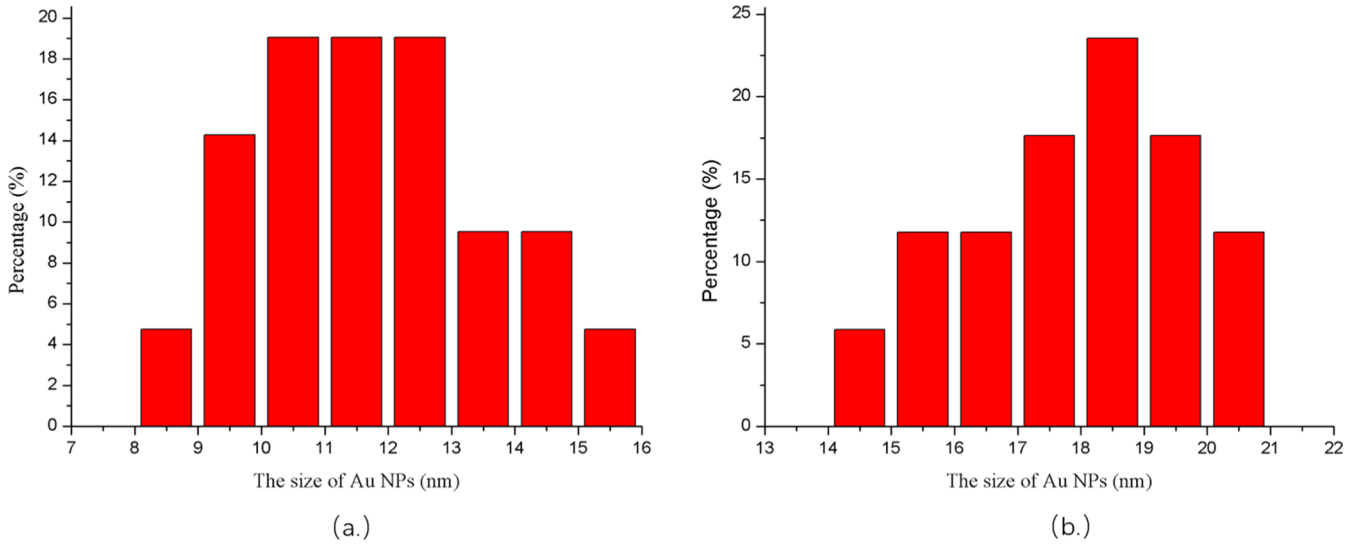

Figure 4. Size distribution of Au NPs of Au/Fe_3O_4 before (a) and after (b) reaction with soot particles.

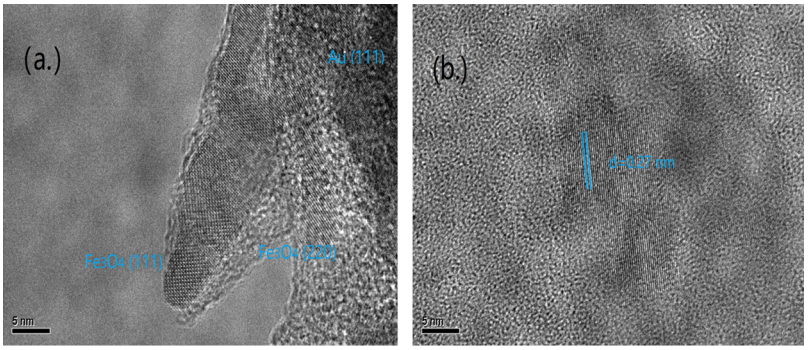

Figure 5. HRTEM images of Au/Fe_3O_4 before (a) and after (b) reaction with soot particles.

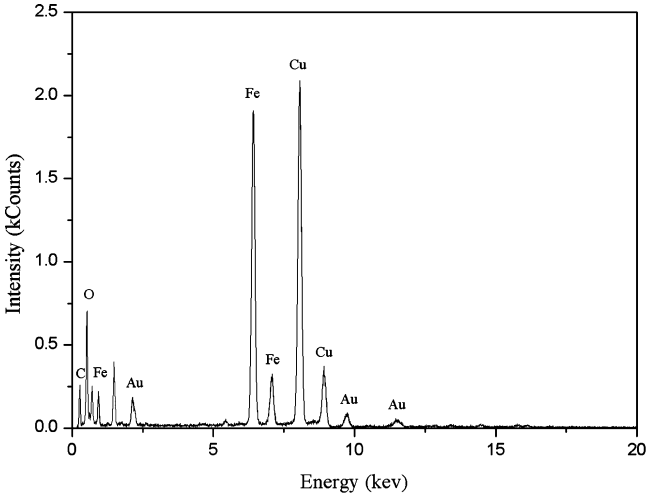

Figure 6. EDS analysis of Au/Fe_3O_4 after the reaction with soot particles.

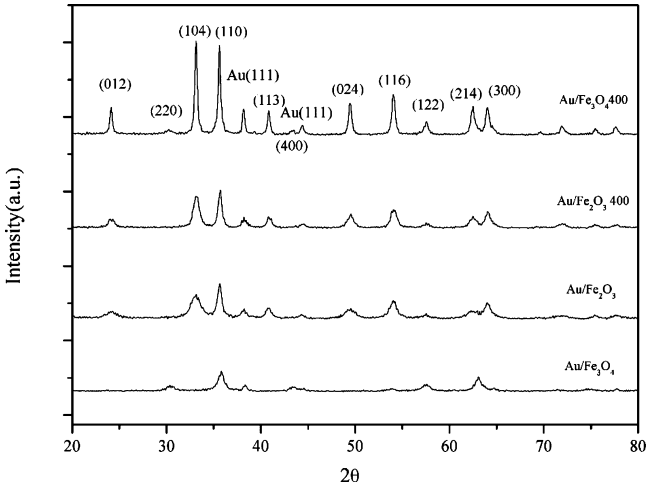

Figure 7. XRD patterns of Au/Fe_2O_3 and Au/Fe_3O_4 before and after the reaction.

the average crystallite size of the catalyst, the smaller the half width of the diffraction peak. After the soot oxidation reaction, the half width of the characteristic diffraction peak of the catalyst becomes smaller, indicating that the size of the catalyst increases. As the temperature increases, the crystallite size of the catalyst becomes larger, which is consistent with the increase in the size of Au NPs measured in the TEM image.

In order to further analyze the changes in the oxidation−reduction properties of the catalysts before and after the reaction with soot particles, XPS tests were carried out on the catalysts Au/Fe_2O_3 and Au/Fe_3O_4 before and after the reaction. Due to the low content of Au NPs in the catalyst, XPS did not detect it. Fe 2p and O 1s photoelectron spectroscopy of the catalysts were mainly tested.

https://doi.org/10.1021/acsomega.1c00619
ACS Omega 2021, 6, 11510−11518

The Fe 2p energy spectrum of the catalysts before and after the reaction is shown in Figure 8. Au/Fe_2O_3 and Au/Fe_3O_4

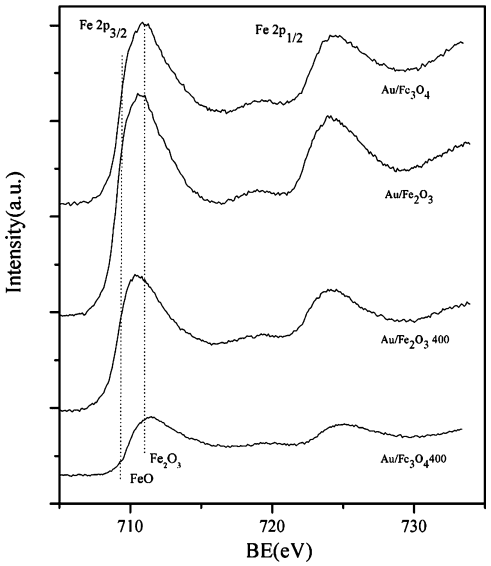

Figure 8. Fe 2p photoelectron spectra of the catalysts before and after the reaction.

have an obvious accompanying peak near 719 eV, indicating the presence of Fe^{3+} on the catalyst surface.[39] Both Fe $2p_{3/2}$ (near 711 eV) and Fe $2p_{1/2}$ (near 724 eV) belong to the characteristic peak of Fe^{3+},[40] and the position of the accompanying peak is 8 eV larger than the peak of Fe $2p_{3/2}$. The peaks that occur near a binding energy (BE) of 709 eV are generally attributed to the ferric divalent Fe^{2+} in the catalyst.[40] As can be seen from the figure, the characteristic peak intensity of Fe^{2+} is small, indicating that there is only a small part of ferric iron in the catalyst, and the iron mainly exists in the form of trivalent.

As can be seen from the XPS spectrum of Fe 2p, the characteristic peak intensity and area of the catalyst after the reaction were smaller than that before the reaction, indicating that the content of ferric iron on the surface of the catalyst decreased with the progress of the reaction, which would lead to the gradual decrease of the catalyst activity.

The O 1s energy spectra of the catalyst Au/Fe_2O_3 and Au/Fe_3O_4 before and after the reaction are shown in Figure 9. The BEs of O 1s are mainly located near 529.3, 531.0, and 532.3 eV. The peaks with BEs between 529.0 and 530.4 eV are mainly attributable to the lattice oxygen (O_{latt}: O^{2-}) on the catalyst surface. The peaks at 531.0−531.4 eV are attributed to the adsorbed oxygen (O_{ads}: O_2^{2-} and O_2^-) on the catalyst surface, while the peaks near 532.2−532.5 eV are the carbonate species or adsorbed water on the catalyst surface.[41] In general, the molar ratio of O_{ads} to O_{latt} is used to measure the reactive oxygen content on the catalyst surface. The larger the ratio, the more active the oxygen components.[42] Compared with the catalyst Au/Fe_3O_4, Au/Fe_2O_3 has a larger molar ratio of adsorbed oxygen to lattice oxygen. In the catalyst activity experiments, it has been proved that Au/Fe_2O_3 has a better catalytic effect on soot oxidation. In addition, after the reaction of Au/Fe_2O_3, carbonate species appeared on the surface, which may be due to the reaction of iron with carbon in the soot particles to form salts.

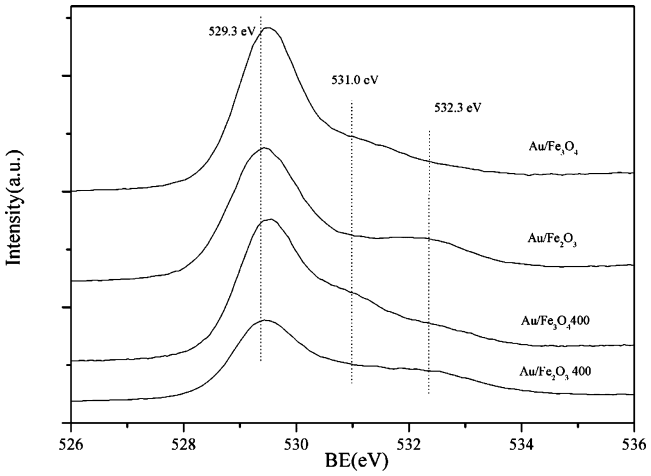

Figure 9. O 1s photoelectron spectra of the catalysts before and after the reaction.

It can also be seen from the XPS spectrum of O 1s that the characteristic peak intensity and area of the catalyst are smaller than before the reaction, indicating that the active oxygen components on the surface of the catalyst gradually decreased after the reaction with soot particles.

The H_2-TPR profiles of the catalysts Au/Fe_2O_3 and Au/Fe_3O_4 before and after the reaction with soot particles are shown in Figure 10. Au/Fe_2O_3 and Au/Fe_3O_4 have obvious

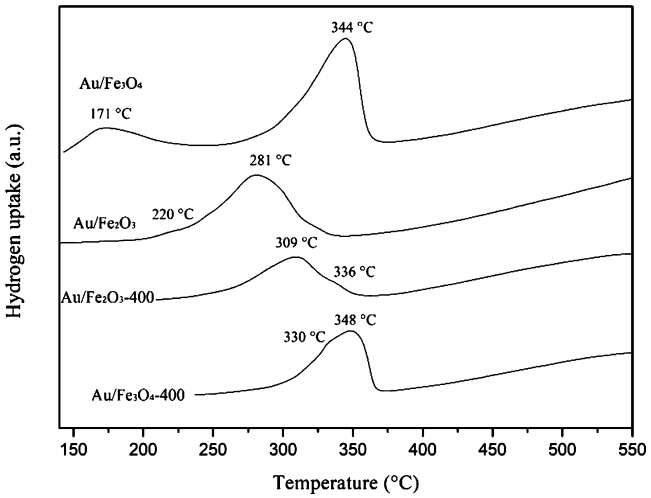

Figure 10. H_2-TPR spectra of the catalysts before and after the reaction.

reduction peaks at 171 and 220 °C before they react with soot particles. According to the literature, the peak at low temperatures is mainly due to the reduction of cationic Au with different valence states.[39] In addition, the preparation method makes it easier to form Au^{3+} species instead of Au^0.[43] The reduction peaks of bulk gold oxide have been reported to appear at about 195 °C.[44] It can be seen from Figure 8 that the first peak is at 165−198 °C, indicating that the reaction between Au and iron oxide promoted its reduction. The reduction reaction in the range of 250−380 °C is related to the a-Fe_2O_3/Fe_3O_4/FeO multiple reduction process.[44] The reduction peaks of the supports Fe_2O_3 and Fe_3O_4 are generally located near 440 °C. After loading Au NPs, the position of the reduction peak was advanced, indicating that Au promoted the

https://doi.org/10.1021/acsomega.1c00619
ACS Omega 2021, 6, 11510−11518

reduction of iron ions to a lower temperature, which was beneficial to improve the oxidation performance of iron-based oxides.

After the catalyst reacted with soot particles, the low-temperature reduction peaks become less intense, which suggests that the reaction between the catalyst and the soot decreased the amount of weakly bounded oxygen. The position of the second main reduction peak shifts backward and the area of the peak decreases, indicating that the oxidation components of iron oxides weakened after reacting with soot particles. For the catalyst Au/Fe_2O_3, its main reduction peak temperature shifts backward from 281 to 309 °C after reacting with soot. For Au/Fe_3O_4, the reduction peak shifts from 344 to 348 °C. Because the stepwise reduction of iron oxides is as follows: $Fe_2O_3 \rightarrow Fe_3O_4 \rightarrow FeO$, in this temperature range, the shift of the peak position after the reaction was mainly caused by the reduction of Fe^{3+}, and it was consistent with the XPS results.

3. CONCLUSIONS

A series of Au/Oxide catalysts were synthesized by the deposition−precipitation method, and their catalytic properties in soot oxidation processes were examined. These transition-metal oxides exhibit excellent soot oxidation activity, especially after loading Au NPs. The catalytic behavior of the catalysts Au/Fe_2O_3 and Au/Fe_3O_4 before and after the reaction with soot particles was emphatically studied. TEM and XRD characterization performed over the Au/Fe_3O_4 catalyst revealed the presence of highly dispersed Au NPs with a size increase from 11 nm in the fresh sample to 17.5 nm in the spent one. Compared with Au/Fe_3O_4, Au/Fe_2O_3 had a better soot catalytic activity mainly due to the larger molar ratio of adsorbed oxygen to lattice oxygen and iron basically in the trivalent state. The H_2-TPR measurement results showed that the strong metal−support interaction between Au NPs and the iron-based oxide could promote the reduction of iron ions and improve its soot oxidation performance. After Au/Fe_2O_3 and Au/Fe_3O_4 reacted with soot particles, the catalysts became more concentrated and the iron in the catalyst was converted from Fe^{3+} to Fe^{2+}. The content of ferric iron and reactive oxygen components on the surface of the catalyst decreases gradually with the progress of the catalytic reaction, resulting in a decrease in catalyst activity.

4. EXPERIMENTAL SECTION

4.1. Catalyst Preparation. The catalysts of transition-metal oxides supported Au NPs were prepared by the deposition−precipitation method. This method can attach all active components to the metal oxide, increase the number of active components, and the size distribution of Au NPs is uniform.

In a typical process, gold chloride hydrate was dissolved in deionized water, and the aqueous solution of $HAuCl_4$ at a concentration of 10 g/L was prepared. Two grams of the commercial metal oxide powder (Fe_2O_3, Fe_3O_4, Co_3O_4, NiO, and CeO_2) was added into 4 mL of the aqueous $HAuCl_4$ solution, further dispersed into 80 mL of deionized water, followed by ultrasonic dispersion for 7 min and then standing for 10 min. About 3.8 g of urea $CO(NH_2)_2$ was added to the mixture to form a slurry. The pH of the slurry was adjusted to 7 by controlling the quality of urea. Then, the suspension was stirred at 80 °C using magnetic force for 3 h and allowed to stand at room temperature for 12 h. The standing solution was centrifuged and filtered, and the powder was washed to neutral using deionized water, then placed in a drying oven, and dried at 80 °C for 6 h. Finally, the dried sample was placed in a tube furnace and heated to 300 °C for 1 h in an atmosphere of 20% oxygen. After natural cooling, the sample was taken out and ground. Thus, the transition-metal oxide loaded with gold NPs was obtained.

In order to obtain the catalysts after the reaction with soot particles, Au/Fe_2O_3 and Au/Fe_3O_4 were mixed and ground with soot particles, respectively, at a mass ratio of 5:1 to obtain their mixture, then, they were placed in a fixed bed reactor and subjected to temperature-controlled oxidation. The mixture was heated at 400 °C for 20 min to obtain the reacted catalysts.

4.2. Catalyst Characterization. In this paper, the changes of morphology, phase structure, and physicochemical properties of the catalysts Au/Fe_2O_3 and Au/Fe_3O_4 before and after the reaction with soot particles were further observed by means of HRTEM, XRD, XPS, and TPR.

HRTEM was used to observe the changes in the morphology and structure of the catalyst before and after the reaction with soot particles, and the average particle size of the gold NPs was calculated. The instrument model used in the experiment was JEM-2011. Before the sample was tested using TEM, the catalyst powder was first dispersed in an acetone solution, followed by ultrasonic treatment for 10 min. Finally, the dispersed suspension was dropped on the ultra-thin copper network for test and analysis.

A high-power powder X-ray diffractometer was used to test and analyze the phase structure of the catalyst and compare the structural changes of the catalyst before and after the reaction with soot particles. The diffractometer used in the experiment was TTRAX-III type produced by Tokyo Rigaku Company. The target source used in the test was the Cu Kα target, the 2θ scanning angle of the catalyst sample was 20−80°, and the scanning rate was 4° min^{-1}.

XPS was used to test and analyze the surface element composition and the main valence state of the catalysts and to compare the change of the valence state of the catalyst before and after the reaction with soot particles. The optoelectronic spectrometer used in the experiment was the model PHI-1600 produced by Elmer Company using Al Ka ($h\nu$ = 1486.6 eV) as the X-ray source with a voltage of 13 kV and a power of 400 W. A carbon C 1s peak (BE = 284.6 eV) was used to calibrate the BE migration, and the test ranges of Fe 2p and O 1s electron BE were 705−735 and 526−536 eV, respectively.

Temperature-programmed reduction with H_2 measurement (H_2-TPR) was performed in a conventional flow apparatus. The sample (100 mg) was pretreated by calcination with N_2 at 300 °C for 1 h and then cooled to room temperature. The gas flow of 10% H_2/N_2 (30 mL min^{-1}) passed the sample in the range of RT to 600 °C at a heating rate of 10 °C min^{-1}.

4.3. Catalyst Activity Evaluation. In order to ensure the consistency of the performance of soot samples, the carbon black Printex-U was used in these experiments to replace the soot particles, which is widely used as a model substance. The average particle size of particles was 25 nm, the volatile content was 5% at 950 °C, and the ash content was less than 0.02%. The catalysts (100 mg) were mixed with soot particles (20 mg) in an agate mortar to the close contact mode by using a spoon. The catalyst activity experiments were carried out on a thermogravimetric analyzer. The mixed samples of the catalyst and soot particles were placed on an aluminum crucible,

https://doi.org/10.1021/acsomega.1c00619
ACS Omega 2021, 6, 11510−11518

heating from room temperature to 800 °C at 10 °C/min. The sample carrier gas was air at a flow rate of 75.0 mL/min, and the equilibrium gas was nitrogen at a flow rate of 25.0 mL/min.

In this paper, the mass change of soot particles before and after the reaction was measured, and the conversion rate of soot particles was calculated, so as to evaluate the catalytic activity of the catalyst. The calculation formula of the conversion rate of soot particles is as follows

$$\eta = \frac{[\text{Soot}]_B - [\text{Soot}]_F}{[\text{Soot}]_B} \times 100\% \quad (1-1)$$

Among them, $[\text{Soot}]_B$ represents the quality of soot particles before reaction and $[\text{Soot}]_F$ represents the quality of soot particles after reaction. In this paper, T_{10}, T_{50}, and T_{90} were used to represent the corresponding temperatures when the conversion rates of soot particles were 10, 50, and 90%, respectively. In addition, T_m was used to represent the characteristic temperature corresponding to the maximum conversion rate of soot particles. When the conversion rate is the same, the smaller the corresponding temperature value, the better the catalytic activity.

AUTHOR INFORMATION

Corresponding Author

Chao Hu − *Advanced Technology Research Institute of Green Building of Anhui Province, Anhui Jianzhu University, Hefei 230601, People's Republic of China; Key Laboratory of Indoor Thermal and Humid Environment, Anhui Jianzhu University, Hefei 230601, People's Republic of China;* orcid.org/0000-0002-6036-0548; Phone: +86 5516 3828252; Email: chaohu@mail.ustc.edu.cn

Authors

Zhenzhen Chen − *Advanced Technology Research Institute of Green Building of Anhui Province, Anhui Jianzhu University, Hefei 230601, People's Republic of China*

Chao Wei − *Advanced Technology Research Institute of Green Building of Anhui Province, Anhui Jianzhu University, Hefei 230601, People's Republic of China*

Xiaokang Wan − *Advanced Technology Research Institute of Green Building of Anhui Province, Anhui Jianzhu University, Hefei 230601, People's Republic of China*

Wenzhi Li − *Department of Thermal Science and Energy Engineering, University of Science and Technology of China, Hefei 230026, People's Republic of China;* orcid.org/0000-0002-7082-5839

Qizhao Lin − *Department of Thermal Science and Energy Engineering, University of Science and Technology of China, Hefei 230026, People's Republic of China*

Complete contact information is available at: https://pubs.acs.org/10.1021/acsomega.1c00619

Notes

The authors declare no competing financial interest.

ACKNOWLEDGMENTS

This work was supported by the Natural Science Foundation of Anhui Province (2008085QE263, 2008085QE206) and the University Natural Science Research Project of Anhui Province (KJ2018JD07, KJ2019A0760). The authors gratefully acknowledge all these supports.

REFERENCES

(1) Schulz, F.; Commodo, M.; Kaiser, K.; De Falco, G.; Minutolo, P.; Meyer, G.; DAnna, A.; Gross, L. Insights into incipient soot formation by atomic force microscopy. *Proc. Combust. Inst.* **2019**, *37*, 885−892.

(2) Rao, C.; Liu, R.; Feng, X.; Shen, J.; Peng, H.; Xu, X.; Fang, X.; Liu, J.; Wang, X. Three-dimensionally ordered macroporous SnO_2-based solid solution catalysts for effective soot oxidation. *Chin. J. Catal.* **2018**, *39*, 1683−1694.

(3) Pu, X.; Cai, Y.; Shi, Y.; Wang, J.; Gu, L.; Tian, J.; Li, W. Diesel particulate filter (DPF) regeneration using non-thermal plasma induced by dielectric barrier discharge. *J. Energy Inst.* **2018**, *91*, 655−667.

(4) Ranji-Burachaloo, H.; Masoomi-Godarzi, S.; Khodadadi, A. A.; Mortazavi, Y. Synergetic effects of plasma and metal oxide catalysts on diesel soot oxidation. *Appl. Catal., B* **2016**, *182*, 74−84.

(5) Wei, Y.; Liu, J.; Zhao, Z.; Duan, A.; Jiang, G. The catalysts of three-dimensionally ordered macroporous $Ce_{1-x}Zr_xO_2$-supported gold nanoparticles for soot combustion: The metal−support interaction. *J. Catal.* **2012**, *287*, 13−29.

(6) Wang, Y.; Arandiyan, H.; Scott, J.; Akia, M.; Dai, H.; Deng, J.; Aguey-Zinsou, K.-F.; Amal, R. High Performance Au−Pd Supported on 3D Hybrid Strontium-Substituted Lanthanum Manganite Perovskite Catalyst for Methane Combustion. *ACS Catal.* **2016**, *6*, 6935−6947.

(7) Miao, S.; Deng, Y. Au−Pt/Co_3O_4 catalyst for methane combustion. *Appl. Catal., B* **2001**, *31*, L1−L4.

(8) Hashmi, A. S. K.; Hutchings, G. J. Gold Catalysis. *Angew. Chem., Int. Ed.* **2006**, *45*, 7896−7936.

(9) Herzing, A. A.; Kiely, C. J.; Carley, A. F.; Landon, P.; Hutchings, G. J. Identification of active gold nanoclusters on iron oxide supports for CO oxidation. *Sci* **2008**, *321*, 1331−1335.

(10) Yu, H.; Dong, F.; Guo, J.; Zhu, B.; Huang, W.; Zhang, S. Gold nanoparticles supported on $LnPO_4$ (Ln = La, Ce) nanorods and nanospheroids as high performance catalysts for CO oxidation. *Mater. Res. Bull.* **2018**, *97*, 411−420.

(11) Van Craenenbroeck, J.; Andreeva, D.; Tabakova, T.; Van Werde, K.; Mullens, J.; Verpoort, F. Spectroscopic Analysis of Au−V-Based Catalysts and Their Activity in the Catalytic Removal of Diesel Soot Particulates. *J. Catal.* **2002**, *209*, 515−527.

(12) Corro, G.; Flores, J. A.; Pacheco-Aguirre, F.; Pal, U.; Bañuelos, F.; Torralba, R.; Olivares-Xometl, O. Effect of the Electronic State of Cu, Ag, and Au on Diesel Soot Abatement: Performance of Cu/ZnO, Ag/ZnO, and Au/ZnO Catalysts. *ACS Omega* **2019**, *4*, 5795−5804.

(13) Wei, Y.; Zhao, Z.; Yu, X.; Jin, B.; Liu, J.; Xu, C.; Duan, A.; Jiang, G.; Ma, S. One-pot synthesis of core−shell Au@$CeO_{2-\delta}$ nanoparticles supported on three-dimensionally ordered macroporous ZrO_2 with enhanced catalytic activity and stability for soot combustion. *Catal. Sci. Technol.* **2013**, *3*, 2958.

(14) Wei, Y.; Zhao, Z.; Liu, J.; Liu, S.; Xu, C.; Duan, A.; Jiang, G. Multifunctional catalysts of three-dimensionally ordered macroporous oxide-supported Au@Pt core−shell nanoparticles with high catalytic activity and stability for soot oxidation. *J. Catal.* **2014**, *317*, 62−74.

(15) Wei, Y.; Zhao, Z.; Jin, B.; Yu, X.; Jiao, J.; Li, K.; Liu, J. Synthesis of AuPt alloy nanoparticles supported on 3D ordered macroporous oxide with enhanced catalytic performance for soot combustion. *Catal. Today* **2015**, *251*, 103−113.

(16) Xiong, J.; Mei, X.; Liu, J.; Wei, Y.; Zhao, Z.; Xie, Z.; Li, J. Efficiently multifunctional catalysts of 3D ordered meso-macroporous $Ce_{0.3}Zr_{0.7}O_2$-supported PdAu@CeO_2 core-shell nanoparticles for soot oxidation: Synergetic effect of Pd-Au-CeO_2 ternary components. *Appl. Catal., B* **2019**, *251*, 247−260.

(17) Wu, Q.; Xiong, J.; Zhang, Y.; Mei, X.; Wei, Y.; Zhao, Z.; Liu, J.; Li, J. Interaction-Induced Self-Assembly of Au@La_2O_3 Core-Shell Nanoparticles on $La_2O_2CO_3$ Nanorods with Enhanced Catalytic Activity and Stability for Soot Oxidation. *ACS Catal.* **2019**, *9*, 3700−3715.

(18) Zhou, X.; Shen, Q.; Yuan, K.; Yang, W.; Chen, Q.; Geng, Z.; Zhang, J.; Shao, X.; Chen, W.; Xu, G.; Yang, X.; Wu, K. Unraveling

Charge State of Supported Au Single-Atoms during CO Oxidation. *J. Am. Chem. Soc.* **2018**, *140*, 554−557.
(19) Ha, H.; Yoon, S.; An, K.; Kim, H. Y. Catalytic CO Oxidation over Au Nanoparticles Supported on CeO_2 Nanocrystals: Effect of the Au−CeO_2 Interface. *ACS Catal.* **2018**, *8*, 11491−11501.
(20) Wang, L.; Zhang, J.; Zhu, Y.; Xu, S.; Wang, C.; Bian, C.; Meng, X.; Xiao, F.-S. Strong Metal−Support Interactions Achieved by Hydroxide-to-Oxide Support Transformation for Preparation of Sinter-Resistant Gold Nanoparticle Catalysts. *ACS Catal.* **2017**, *7*, 7461−7465.
(21) Mitsudome, T.; Yamamoto, M.; Maeno, Z.; Mizugaki, T.; Jitsukawa, K.; Kaneda, K. One-step Synthesis of Core-Gold/Shell-Ceria Nanomaterial and Its Catalysis for Highly Selective Semihydrogenation of Alkynes. *J. Am. Chem. Soc.* **2015**, *137*, 13452−13455.
(22) Yang, H.; Deng, J.; Xie, S.; Jiang, Y.; Dai, H.; Au, C. T. Au/MnOx/3DOM SiO_2: Highly active catalysts for toluene oxidation. *Appl. Catal., A* **2015**, *507*, 139−148.
(23) Widmann, D.; Liu, Y.; Schüth, F.; Behm, R. J. Support effects in the Au-catalyzed CO oxidation−Correlation between activity, oxygen storage capacity, and support reducibility. *J. Catal.* **2010**, *276*, 292−305.
(24) Carabineiro, S. A. C.; Chen, X.; Martynyuk, O.; Bogdanchikova, N.; Avalos-Borja, M.; Pestryakov, A.; Tavares, P. B.; Órfão, J. J. M.; Pereira, M. F. R.; Figueiredo, J. L. Gold supported on metal oxides for volatile organic compounds total oxidation. *Catal. Today* **2015**, *244*, 103−114.
(25) Ousmane, M.; Liotta, L. F.; Carlo, G. D.; Pantaleo, G.; Venezia, A. M.; Deganello, G.; Retailleau, L.; Boreave, A.; Giroir-Fendler, A. Supported Au catalysts for low-temperature abatement of propene and toluene, as model VOCs: Support effect. *Appl. Catal., B* **2011**, *101*, 629−637.
(26) Gao, Y.; Duan, A.; Liu, S.; Wu, X.; Liu, W.; Li, M.; Chen, S.; Wang, X.; Weng, D. Study of Ag/$Ce_xNd_{1-x}O_2$ nanocubes as soot oxidation catalysts for gasoline particulate filters: Balancing catalyst activity and stability by Nd doping. *Appl. Catal., B* **2017**, *203*, 116−126.
(27) Huang, J.; He, S.; Goodsell, J. L.; Mulcahy, J. R.; Guo, W.; Angerhofer, A.; Wei, W. D. Manipulating Atomic Structures at the Au/TiO_2 Interface for O_2 Activation. *J. Am. Chem. Soc.* **2020**, *142*, 6456−6460.
(28) Portillo-Vélez, N. S.; Zanella, R. Comparative study of transition metal (Mn, Fe or Co) catalysts supported on titania: Effect of Au nanoparticles addition towards CO oxidation and soot combustion reactions. *Chem. Eng. J.* **2020**, *385*, 123848.
(29) Mukherjee, D.; Reddy, B. M. Noble metal-free CeO_2-based mixed oxides for CO and soot oxidation. *Catal. Today* **2018**, *309*, 227−235.
(30) Krishna, K.; Bueno-López, A.; Makkee, M.; Moulijn, J. A. Potential rare earth modified CeO_2 catalysts for soot oxidation: I. Characterisation and catalytic activity with O_2. *Appl. Catal., B* **2007**, *75*, 189−200.
(31) Li, Q.; Wang, X.; Xin, Y.; Zhang, Z.; Zhang, Y.; Hao, C.; Meng, M.; Zheng, L.; Zheng, L. A unified intermediate and mechanism for soot combustion on potassium-supported oxides. *Sci. Rep.* **2014**, *4*, 4725.
(32) Lin, Y.; Zhu, B.; Chen, J.; Wu, J.; Lu, K.; Gu, M.; Chu, H. Study of soot functional groups and morphological characteristics in laminar coflow methane and ethylene diffusion flames with hydrogen addition. *Fuel* **2020**, *279*, 118474.
(33) Kim, T.-S.; Kim, J.; Song, H. C.; Kim, D.; Jeong, B.; Lee, J.; Shin, J. W.; Ryoo, R.; Park, J. Y. Catalytic Synergy on PtNi Bimetal Catalysts Driven by Interfacial Intermediate Structures. *ACS Catal.* **2020**, *10*, 10459−10467.
(34) Kim, J.; Park, W. H.; Doh, W. H.; Lee, S. W.; Noh, M. C.; Gallet, J.-J.; Bournel, F.; Kondoh, H.; Mase, K.; Jung, Y.; Mun, B. S.; Park, J. Y. Adsorbate-driven reactive interfacial Pt-NiO_{1-x} nanostructure formation on the Pt_3Ni (111) alloy surface. *Sci. Adv.* **2018**, *4*, No. eaat3151.
(35) Guo, J.; Yang, Y.; Yu, W.; Dong, X.; Wang, J.; Liu, G.; Wang, T. Synthesis of α-Fe_2O_3, Fe_3O_4 and Fe_2N magnetic hollow nanofibers as anode materials for Li-ion batteries. *RSC Adv.* **2016**, *6*, 111447−111456.
(36) Yu, H.; Chen, M.; Rice, P. M.; Wang, S. X.; White, R. L.; Sun, S. Dumbbell-like bifunctional Au−Fe_3O_4 nanoparticles. *Nano Lett.* **2005**, *5*, 379−382.
(37) Zeng, Q. Z.; Ma, S. Y.; Jin, W. X.; Yang, H. M.; Chen, H.; Ge, Q.; Ma, L. Hydrothermal synthesis of monodisperse α-Fe_2O_3 hollow microspheroids and their high gas-sensing properties. *J. Alloys Compd.* **2017**, *705*, 427−437.
(38) Schimanke, G.; Martin, M. In situ XRD study of the phase transition of nanocrystalline maghemite (γ-Fe_2O_3) to hematite (α-Fe_2O_3). *Solid State Ionics* **2000**, *136*−*137*, 1235−1240.
(39) Ayastuy, J. L.; Gurbani, A.; Gutiérrez-Ortiz, M. A. Effect of calcination temperature on catalytic properties of Au/Fe_2O_3 catalysts in CO-PROX. *Int. J. Hydrogen Energy* **2016**, *41*, 19546−19555.
(40) Yamashita, T.; Hayes, P. Analysis of XPS spectra of Fe^{2+} and Fe^{3+} ions in oxide materials. *Appl. Surf. Sci.* **2008**, *254*, 2441−2449.
(41) Tang, X.; Li, Y.; Huang, X.; Xu, Y.; Zhu, H.; Wang, J.; Shen, W. MnOx−CeO_2 mixed oxide catalysts for complete oxidation of formaldehyde: effect of preparation method and calcination temperature. *Appl. Catal., B* **2006**, *62*, 265−273.
(42) Li, J.; Liang, X.; Xu, S.; Hao, J. Catalytic performance of manganese cobalt oxides on methane combustion at low temperature. *Appl. Catal., B* **2009**, *90*, 307−312.
(43) Zanella, R.; Delannoy, L.; Louis, C. Mechanism of deposition of gold precursors onto TiO_2 during the preparation by cation adsorption and deposition−precipitation with NaOH and urea. *Appl. Catal., A* **2005**, *291*, 62−72.
(44) Venugopal, A.; Scurrell, M. S. Low temperature reductive pretreatment of Au/Fe_2O_3 catalysts, TPR/TPO studies and behaviour in the water−gas shift reaction. *Appl. Catal., A* **2004**, *258*, 241−249.

https://doi.org/10.1021/acsomega.1c00619
ACS Omega 2021, 6, 11510−11518